

# Improvement on Corrosion Resistance and Biocompatibility of ZK60 Magnesium Alloy by Carboxyl Ion Implantation

Xian Wei, Su-Jie Ma, Pin-Duo Liu, Zhi-Cheng Li, Xu-Biao Peng, Rong-Ping Deng, and Qing Zhao\*  
*Beijing institute of technology*

Magnesium alloys have been considered to be potential biocompatible metallic materials. Further improvement on the anti-corrosion is expected to make this type of materials more suitable for biomedical applications in the fields of orthopedics, cardiovascular surgery and others. In this paper, we introduce a method of carboxyl ion ( $\text{COOH}^+$ ) implantation to reduce the degradation of ZK60 Mg alloy and improve its functionality in physiological environment. X-ray photoelectron spectroscopy (XPS) and atomic force microscopy (AFM) experiments show the formation of a smooth layer containing carboxylic group, carbonate, metal oxides and hydroxides on the ion implanted alloy surface. Corrosion experiments and *in vitro* cytotoxicity tests demonstrate that the ion implantation treatment can both reduce the corrosion rate and improve the biocompatibility of the alloy. The promising results indicate that organic functional group ion implantation may be a practical method of improving the biological and corrosion properties of magnesium alloys.

PACS numbers: 03.75.Lm, 03.75.Mn, 67.85.Hj  
 Keywords:

## I. INTRODUCTION

Because of their mechanical and biocompatible properties, magnesium alloys are promising materials for applications in medical fields [7, 22]. Mg alloys can provide effectively mechanical support for the injured tissue during healing period and can be completely biodegraded in the human body after being cured without a removal surgery [21, 49]. Magnesium alloys also present high strength to weight ratio and excellent mechanical properties. The densities of magnesium alloys range from 1.74 to 2.0 g/cm<sup>3</sup> and the elastic moduli are from 41 to 45 GPa which are closer to the bones than that of the Ti-based alloys (4.4-4.5 g/cm<sup>3</sup> and 110-117 GPa) and stainless steels (7.9-8.1 g/cm<sup>3</sup> and 189-205 GPa) [43]. In addition, the released Mg ions are indispensable in many biological processes and have positive effect on the osteoblast adhesion and proliferation [13, 15, 50]. Despite possessing these promising characteristics, rapid and uncontrollable corrosion rate has restricted their applications in biomedical field. The fast corrosion rate may lead to the failure of mechanical support, excessive corrosion products, and formation of local alkaline environment. In order to improve the anticorrosion of Mg alloys, various methods have been proposed, including alloying, coating, and surface treatment such as anodization, physical/chemical vapor deposition. However, these methods have drawbacks. For example, the alloying method may improve the anticorrosion property by compromising the mechanical property and the biocompatibility, while the coating method may have inadequate bonding between the coating layer to the alloy [3].

The method of ion implantation is a surface treatment by introducing foreign ions to form a stable functional layer on the material surface in order to reduce the corrosion rate and improve the biocompatibility of magnesium alloys. The energetic ions directly implanted into the alloy surface do not

change the size and shape of the material objects. Besides, the implantation process is clean and environmentally friendly. A number of literatures have been reported the positive effects of ion implantation on Mg alloys. Tao et al. [44] grafted Gd into ZK60 Mg alloy by ion implantation and demonstrated that the corrosion resistance, surface hardness and modulus of the Gd implanted magnesium alloy are enhanced. Liu et al. [28] revealed that the cytocompatibility of MC3T3-E1 cells is improved and the corrosion behavior is comparable after Zn ion implantation and deposition of the Mg-1Ca alloy. Jamesh et al. [20] introduced Zr, O, and Zr & O ions into the ZK60 Mg alloy surface by plasma immersion ion implantation. Their work showed the enhanced corrosion resistance of the treated alloy. However, excessive amounts of metal ions in human body could cause toxic effects. Li et al. had reported that cerium (Ce), praseodymium (Pr) and yttrium (Y) can induce rigorous hepatotoxicity when exceeding the allowable dosage [24]. Thus, the elements with no or low toxicity and larger tolerance dosage should be taken into consideration for ion implantation.

Organic functional carboxylic ions ( $\text{COOH}^+$ ) are less toxic as compared to metallic ions and have presented excellent biosafety and biocompatibility. As reported in the previous studies [23, 54],  $\text{COOH}^+$  implantation leads to much better cell attachment and proliferation on the surface of polypropylene and multiwalled carbon nanotubes. Carboxylic ion implantation also improves the catalytic activity of indium tin oxide electrode which has many applications in new biosensors and biofuel cell [14, 25, 26]. However, to the best of our knowledge, there is little report about the corrosion resistance and the biocompatibility of  $\text{COOH}^+$ -implanted Mg alloys. In this paper, we implant the carboxylic ion into the ZK60 alloy surface with doses of  $1 \times 10^{16}$  and  $5 \times 10^{16}$  ions/cm<sup>2</sup> at the energy of 200 KeV. We identify the surface chemical structure of treated samples by means of X-ray photoelectron spectroscopy (XPS) and atomic force microscopy (AFM). The mechanical performance is measured by Nano indenter. The corrosion property is tested by electrochemical and immersion assays. And the biocompatibility is investigated by cell viability assay *in vitro*.

\*The corresponding author Email: qzhaoyuping@bit.edu.cn

## II. EXPERIMENTAL DETAILS

### A. Ion implantation and surface characterization

The ZK60 Mg alloy with the chemical contents of 5.5wt.% Zn and 0.6wt.% Zr was cut into  $10\text{mm} \times 10\text{mm} \times 2\text{mm}$  chips. Prior to ion implantation, samples were ground by SiC sandpapers up to 3000 grit and then rinsed with consecutive solutions of acetone, absolute ethanol, distilled water in ultrasonic cleaner, respectively. The samples were finally dried in air. Carboxy ion ( $\text{COOH}^+$ ) implantation was carried out with the doses of  $1 \times 10^{16}$  and  $5 \times 10^{16}$  ions/cm<sup>2</sup> using an ion implanter that was equipped with formic acid feeding for ion source at an extraction voltage of 200 KV and a vacuum of  $10^{-3}$  Pa.  $\text{COOH}^+$  ions were identified by mass spectrometry. The ions were implanted into the ZK60 sample with the ion current density less than  $0.01 \text{ A/cm}^2$ .

The X-ray photoelectron spectroscopy (XPS, PHI Quantera II, Ulvac-Phi Inc.) was used to determine the elemental depth profile and the surface chemical compositions of the treated samples. The sputtering rate was approximately 25.8 nm/min based on the  $\text{SiO}_2$  reference. The morphology and roughness of the untreated and the implanted samples are characterized by Atomic force microscopy (AFM, MFP-3D-SA, Asylum Research, USA). Additionally, Nano Indenter (XP, MTS Systems Corporation, USA) was used to study the change of surface mechanical properties of the samples after ion implantation.

### B. Electrochemical tests

The electrochemical workstation was utilized to determine the electrochemical corrosion properties. The tests were conducted at the temperature of  $37^\circ\text{C}$  using a classical three electrode system with a platinum electrode as the counter electrode, a saturated calomel electrode (SCE) as the reference electrode, and the tested sample as the working electrode. The sample with the exposed area of  $1 \text{ cm}^2$  was soaked in Hank's solution. The constituents of Hank's solution were NaCl 8.00 g/L, KCl 0.40 g/L,  $\text{CaCl}_2$  0.14 g/L,  $\text{MgCl}_2 \cdot 6\text{H}_2\text{O}$  0.10 g/L,  $\text{MgSO}_4 \cdot 7\text{H}_2\text{O}$  0.10 g/L,  $\text{KH}_2\text{PO}_4$  0.06 g/L,  $\text{Na}_2\text{HPO}_4 \cdot 2\text{H}_2\text{O}$  0.06 g/L,  $\text{NaHCO}_3$  0.35 g/L, and glucose 1.00 g/L. The electrochemical impedance spectroscopy (EIS) was performed with scanning frequency ranged from 100 kHz to 100 mHz at 5 mV amplitude perturbation. And the potentiodynamic polarization tests were conducted at a scanning rate of 1 mV/s. The corrosion current density ( $I_{corr}$ ) were calculated by analyzing the Tafel extrapolation to the cathodic and anodic part of the polarization curves.

### C. Immersion tests

The immersion tests were conducted in Hank's solution with volume to area ratio of  $20 \text{ mL/cm}^2$  at  $37^\circ\text{C}$  depending on ASTM-G31-72 [18]. The weight loss, pH value, and ion concentration were recorded at each time node. After immersion for 1, 3 and 7 days, the corroded surface was cleaned

with chromic acid, gently rinsed by distilled water, and then dried in open air. The releases of magnesium, calcium, and phosphate species were evaluated using inductively coupled plasma atomic emission spectrometry (ICP-OES, 725-ES, Agilent, USA). The surface morphology of each corroded sample was analyzed by scanning electron microscopy (SEM, S-4800, Hitachi, Japan).

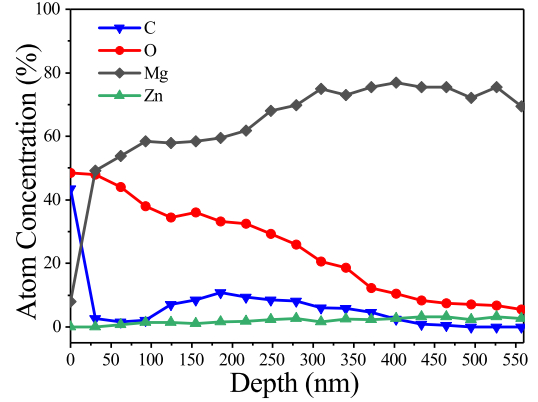


FIG. 1: The elemental depth profiles of the treated sample with dose of  $5 \times 10^{16} \text{ COOH}^+/\text{cm}^2$  by XPS.

### D. In vitro cytotoxicity tests

The osteoblast MC3T3-E1 mice cells were acquired from American Type Culture Collection (ATCC) and used to test the negative effect on cell viability with an indirect method. The cells were cultured in Dulbecco's Modified Eagle's Medium (DMEM, Gibco) along with 10% fetal bovine serum (FBS) at  $37^\circ\text{C}$  in a humidified atmosphere of 5%  $\text{CO}_2$ . Samples were sterilized under ultraviolet radiation for 2 hrs prior to the test. The extracts were prepared by culturing the specimens in the serum free cell culture medium with the extraction ratio of  $1.25 \text{ cm}^2/\text{ml}$  in the incubator with 5%  $\text{CO}_2$  at  $37^\circ\text{C}$  for 72 hrs. The supernatant fluid was withdrawn, centrifuged, and then refrigerated at  $4^\circ\text{C}$  for the test. MC3T3-E1 cells were seeded in 96-well culture plate with a density of  $1 \times 10^3$  cells per well. After the incubation for 24 hrs to allow attachment, the medium was replaced by the extracts from the untreated and the treated ZK60 Mg alloys adding with 10% FBS. The control group was normal DMEM medium with 10% FBS. After incubation for 1 and 3 days, each well was added by  $10 \mu\text{L}$  MTT, and then cultured for another 4 hrs. Then  $150 \mu\text{L}$  dimethyl sulfoxide was added in each well to dissolve the formed formazan crystals. The absorbance peak at 490 nm was observed by the microplate reader (Cytation3, Bio-Teh, USA). In the end, the cell viability was computed as follows:

$$\text{Viability} = \frac{OD_{\text{sample}}}{OD_{\text{control}}} \times 100\% \quad (1)$$

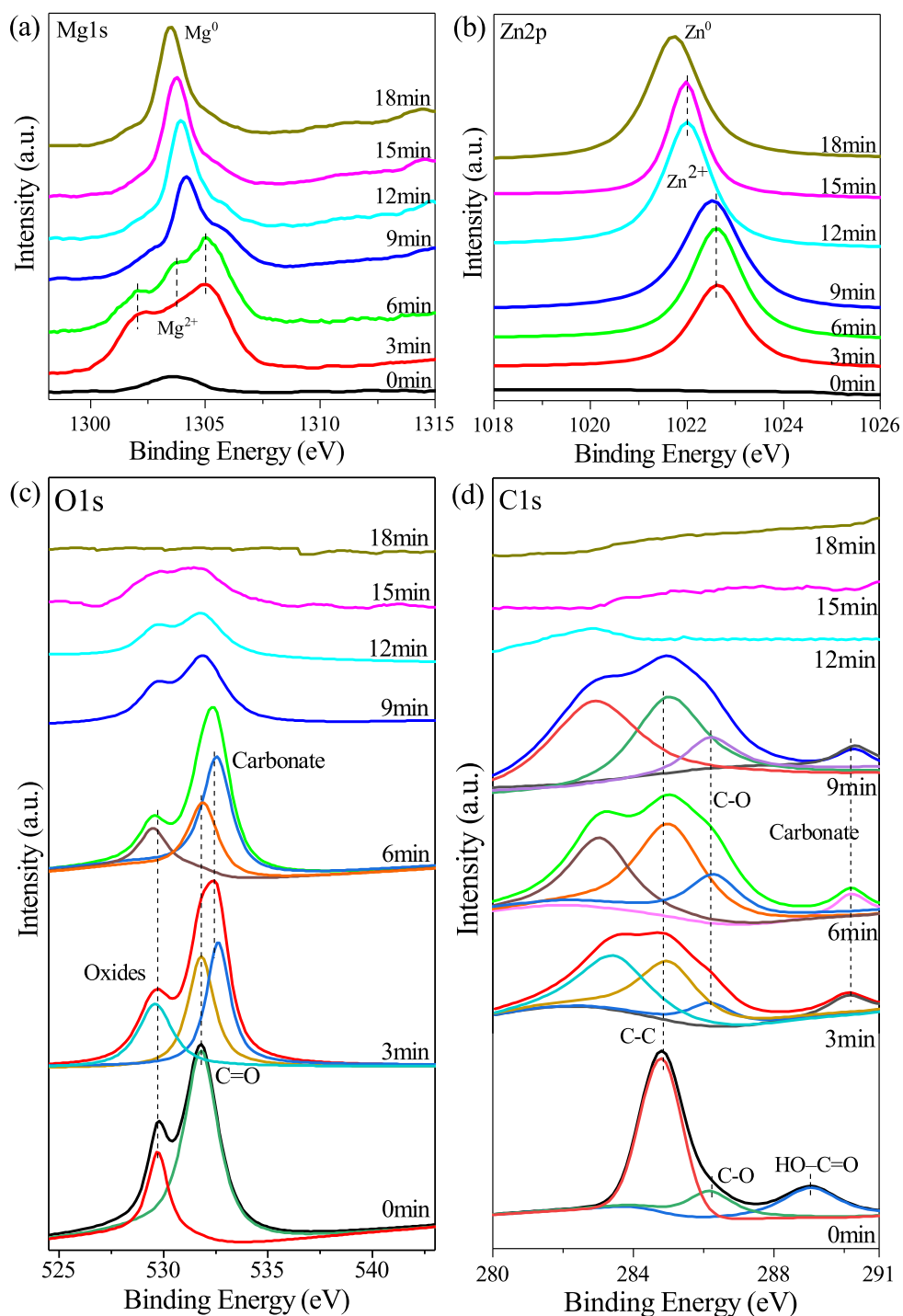


FIG. 2: High-resolution XPS (a) Mg 1s, (b) Zn 2p, (c) O 1s, and (d) C 1s spectra of the treated sample with dose of  $5 \times 10^{16}$  COOH<sup>+</sup>/cm<sup>2</sup> at different sputtering time.

### E. Statistical analysis

The data in this work expressed as mean  $\pm$  standard deviations were analyzed by one-way analysis of variance (ANOVA). Statistical analyses were operated using IBM SPSS Statistics 20.0 for Windows Software (IBM Inc., Ar-

monk, USA) and  $P < 0.05$  reflected statistical significant.

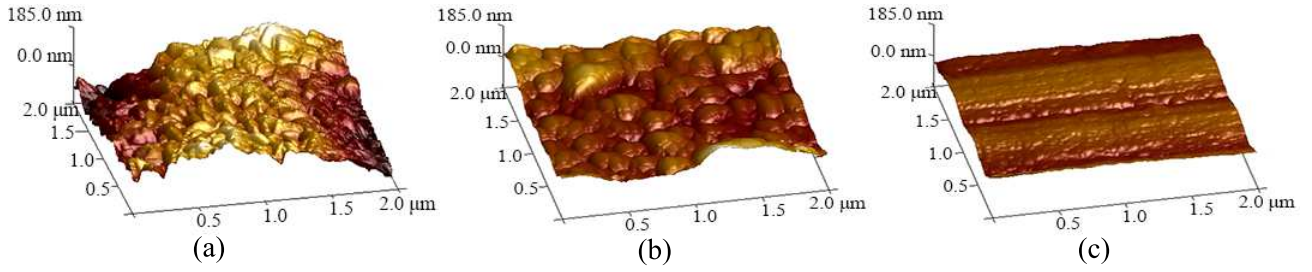


FIG. 3: Surface morphology of the samples observed by AFM: (a) untreated sample, (b) implanted sample with dose of  $1 \times 10^{16}$  ions/cm<sup>2</sup>, and (c) implanted sample with dose of  $5 \times 10^{16}$  ions/cm<sup>2</sup>.

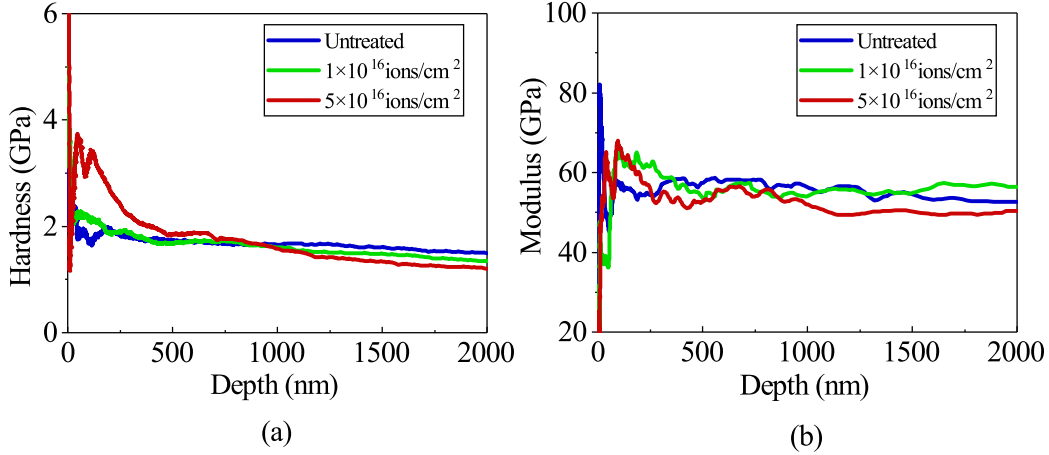


FIG. 4: The hardness (a) and elastic modulus values (b) acquired from the untreated and the treated samples.

### III. RESULTS

#### A. Surface characterization

Fig. 1 shows the XPS depth profile of the treated sample which is implanted by  $\text{COOH}^+$  ions with the dose of  $5 \times 10^{16}$  ions/cm<sup>2</sup>. The magnesium concentration increases gradually with the sputtering depth while the reverse trend is found for oxygen. The concentration of carbon is about 43.5% when the sputtering begins, then drops sharply to 3% at a depth of 25 nm. This change may be due to the air-exposed surface of the sample. Subsequently, the concentration of carbon increases to approximately 11% with sputtering depth of nearly 185 nm. Both oxygen and carbon concentrations decrease to low levels at the depth exceeding 465 nm, which indicates the formation of carboxylic-containing layer on the surface. The high-resolution XPS spectra for Mg 1s, Zn 2p, O 1s, and C 1s regions of the treated sample with dose of  $5 \times 10^{16}$   $\text{COOH}^+$ /cm<sup>2</sup> are depicted in Fig. 2. All the peak positions are calibrated with the C1s adventitious peak (binding energy of 284.8 eV) [46]. The Mg 1s spectrum is deconvoluted into three peaks at the beginning of sputtering, which signifies the formation of oxide, hydroxide, and carbonate in the top surface layer. As the sputtering time continues, those three peaks gradually convert to one peak corresponding to MgO. Finally the Mg 1s peak shifts to low binding energy, which indicates that Mg compounds turn steadily to the metallic state

(Mg<sup>0</sup>). As shown in Fig. 2(b), peak positions at 1022.0 eV and 1022.62 eV are assigned to the oxide and hydroxide of Zn respectively [4]. The binding energy of Zn 2p peak exhibits a decreasing trend which indicates that Zn changes from its oxidized/hydroxy state to the metallic state. The C 1s spectrum is deconvoluted into three peaks at the beginning of the sputtering time, including the adventitious carbon (C-C, 284.8 eV), the hydroxyl carbon (C-O, 286.17 eV), and the carboxylate carbon (HO-C=O, 289.0 eV), which indicates that the successful grafting of carboxylic functional group on the surface of ZK60 magnesium alloys. Subsequently, the intensity of C changes significantly with increasing in depth. The peaks near 290.0 eV is associated with the formation of carbonates, which is consistent with the Mg peak [10, 30]. For the oxygen states, the O 1s spectrum is mainly separated into three peaks at the beginning of sputtering, which correspond to oxide, carbonate, and carbonyl groups, respectively. The presence of carbon and oxygen confirms that the carboxylic functional group is successfully grafted on the alloy surface to form various compounds, such as carbonates, metal oxides and hydroxides. The formation of the functional layer on top of the Mg substrate can provide to protect the alloy from corrosion by the external aggressive solution.

Fig. 3 shows the surface 3D topography of the untreated and the treated samples observed with atomic force microscopy (AFM). The surface morphology of the untreated sample is quite rough with obvious convex. The compact,

uniform and relatively smooth surfaces form after the implantation of  $\text{COOH}^+$  ions on the untreated sample. The AFM images are taken with the area of  $2 \times 2 \mu\text{m}$ . The corresponding root-mean-square (RMS) roughness values are calculated. The RMS value of the untreated sample is 52.8 nm, whereas RMS values are significantly lower for the treated samples (41.7 nm for the treated sample with dose of  $1 \times 10^{16}$  ions/cm<sup>2</sup>, 18.9 nm with dose of  $5 \times 10^{16}$  ions/cm<sup>2</sup>). As the implantation dose increased from  $1 \times 10^{16}$  to  $5 \times 10^{16}$  ions/cm<sup>2</sup>, the surface tends to be much smoother which could be attributed to the surface restructure at the sputtering effect of ion beam bombardment and the energy impact during the implantation process [19, 47, 53]. Most previous studies have reported that evident smooth surface is observed after the ion implantation [6, 32, 56]. Jamesh et al. demonstrated that the WE43 Mg alloy surface is smoother after Si ion implantation [19]. Wan et al. also indicated that the surface of sample treated by oxygen ion implantation appears more homogeneous and smoother [47]. The effect of carboxylic ion implantation on the surface morphology is obvious, which also has impact on the corrosion properties of the ZK60 Mg alloy. Generally, the potential difference between the concave and convex is less for the smoother surface, which corresponds to more resistant to corrosion [17, 27, 36]. Therefore, the corrosion rate of ZK60 Mg alloy is expected to be reduced after  $\text{COOH}^+$  ions implantation.

### B. Mechanical property

The measurement results of the hardness and the elastic modulus for the untreated and the ion implanted samples are shown in Fig. 4. There are no significant changes in the hardness and the modulus from the outer layer to the inner layers on the untreated samples, while the surface up to about 465 nm on the ion implanted samples show higher values of the hardness and the elastic modulus. The hardness and elastic modulus of all the treated samples are larger than those of the bare plate on the top layer and then tend to be stable in deeper indentation depth. This suggests that ion implantation improves the mechanical performance of the ZK60 magnesium alloy [34, 55].

### C. Corrosion performance

Fig. 5 shows the potentiodynamic polarization measurement results for samples soaked in Hank's solution at 37°C. The electrochemical parameters such as corrosion potential ( $E_{corr}$ ) and corrosion current density ( $I_{corr}$ ) are obtained by the Tafel extrapolation and listed in Table I. The  $I_{corr}$  attributes lower values for the treated samples compared with the untreated one. The corrosion current density of the implanted samples decreases with increasing the  $\text{COOH}^+$  ion implantation dose. The  $I_{corr}$  of untreated sample displays nearly 9 times higher than the treated sample with  $5 \times 10^{16}$  ions/cm<sup>2</sup>, 6 times larger than the sample with  $1 \times 10^{16}$  ions/cm<sup>2</sup>. Generally, more negative corrosion current density corresponds to lower corrosion rate [9, 52]. The results of potentiody-

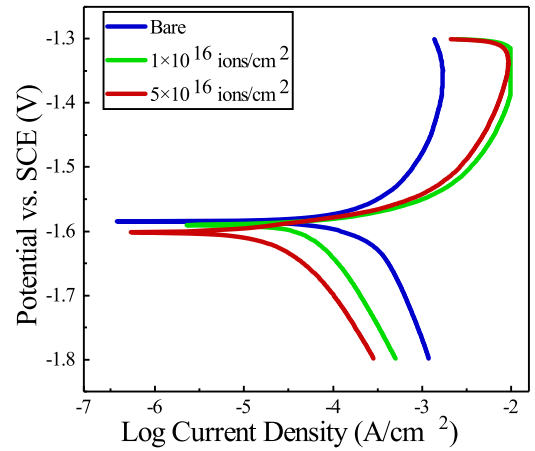


FIG. 5: The potentiodynamic polarization curves of the untreated and treated samples in Hank's solution.

TABLE I: Corrosion parameters calculated from the potentiodynamic polarization curves.

Doses(ions/cm <sup>2</sup> )	$E_{corr}$ (V)	$i_{corr}$ (A/cm <sup>2</sup> )
0	-1.585	$2.9194 \times 10^{-4}$
$1 \times 10^{16}$	-1.59	$4.9799 \times 10^{-5}$
$5 \times 10^{16}$	-1.601	$3.3245 \times 10^{-5}$

amic polarization reveal that the samples have better anti-corrosion performance after  $\text{COOH}^+$  ions implantation. This can be attributed to the formation of functional layer containing carboxylic group, carbonates, metal oxides and hydroxides, which provides a barrier to reduce the corrosion of ZK60 magnesium alloy.

The electrochemical impedance spectroscopy (EIS) is also employed to analyze the corrosion property of the electrode system. Fig. 6 shows the corresponding Nyquist plot and Bode plots, including impedance versus frequency and phase angle versus frequency. As shown in Fig. 6(a), two capacitive loops are observed at high and medium frequencies. They are distinguishable for the treated sample, while almost overlapped for the untreated sample. The diameter of the capacitive semicircle is significantly larger with the dose of  $5 \times 10^{16}$   $\text{COOH}^+$ /cm<sup>2</sup> than with the dose of  $1 \times 10^{16}$   $\text{COOH}^+$ /cm<sup>2</sup>. For the untreated sample, the diameter becomes very small. As reported in literatures [35, 39], capacitive loop at high frequency region is related to the property of the coating and the charge transfer process, and the capacitive loop at low frequency region is associated with the mass transfer process. The formations of carboxylic group, carbonates, metal oxides and hydroxides on the surface of the treated sample act as coating to protect the ZK60 alloy from corrosion. Therefore, the anti-corrosion performance is enhanced for the  $\text{COOH}^+$  ion implanted ZK60 Mg alloy.

The Bode impedance plots of the untreated and the treated samples are shown in Fig. 6(c). The impedances of the treated samples are all higher than the untreated sample at the lower frequency regions, whereas they are almost indistinguishable in higher frequency regions. At the frequency of 100 mHz, measured impedance value of the treated sample with dose of

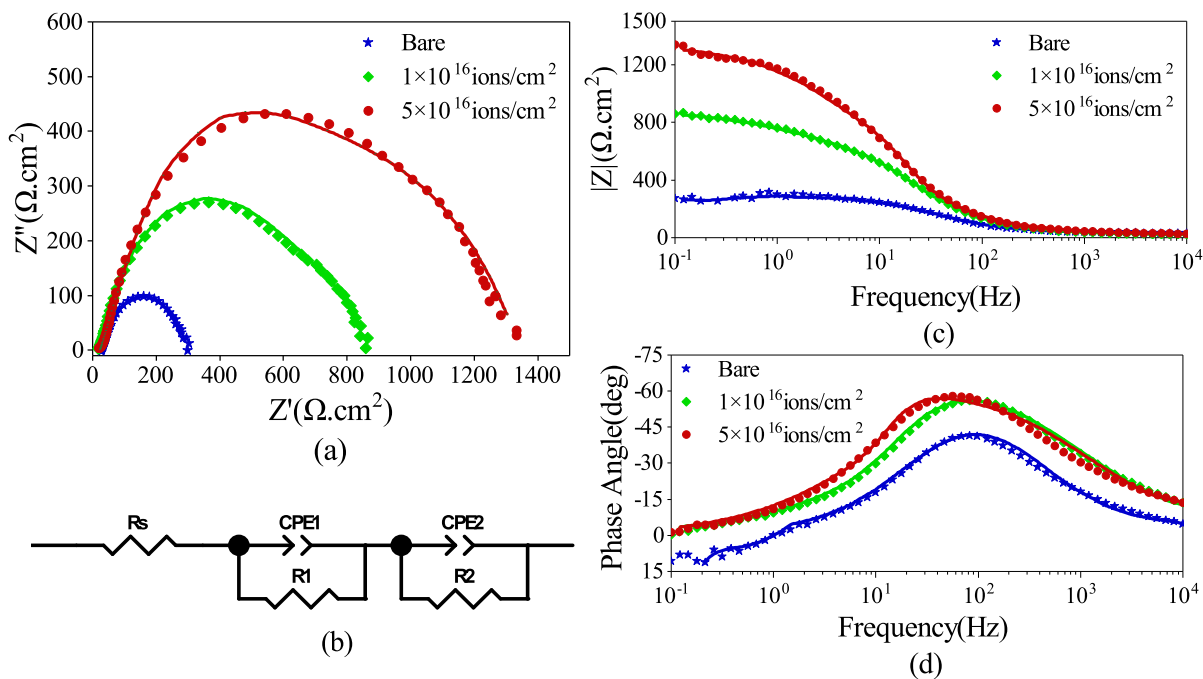


FIG. 6: EIS curve (scatter plot) and model fitting curve (solid line) of samples: (a) Nyquist plot, (b) Equivalent circuit of samples with and without implantation, (c) Bode plot of impedance versus frequency, and (d) Bode plot of phase angle versus frequency.

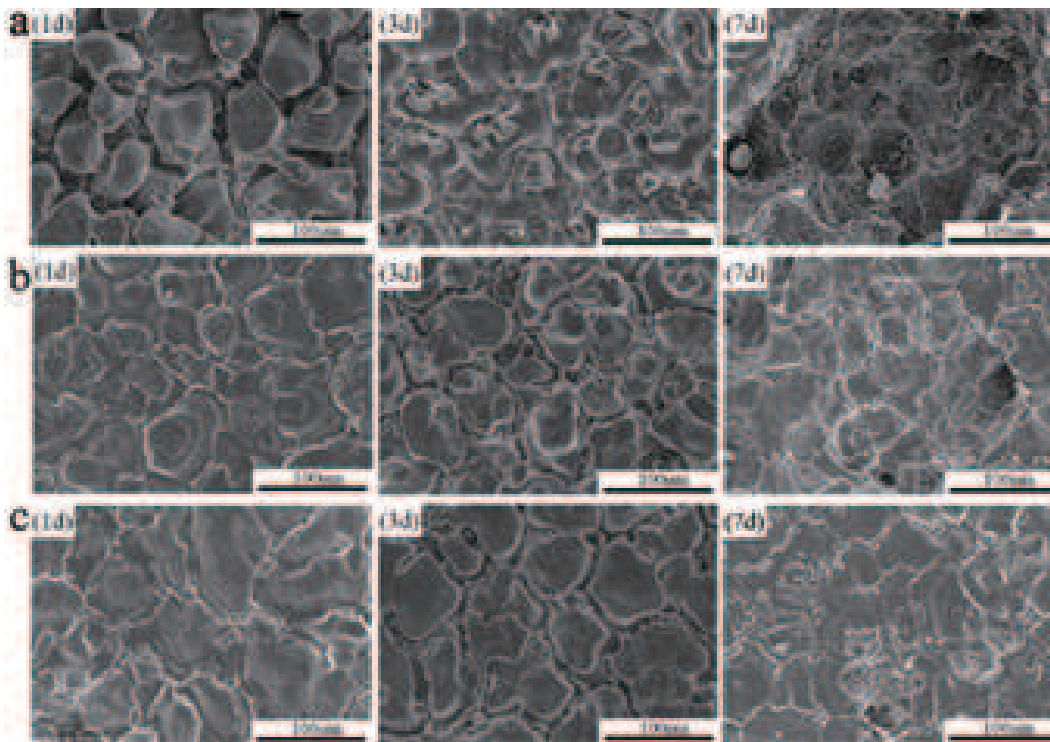


FIG. 7: Surface morphology of samples during different immersion time. Group a the untreated sample, group b the treated sample with dose of  $1 \times 10^{16}$  ions/cm<sup>2</sup>, and group c the treated sample with dose of  $5 \times 10^{16}$  ions/cm<sup>2</sup>.

$5 \times 10^{16}$  ions/cm<sup>2</sup> is the impedance five times higher than that of the untreated sample, and three times higher impedance for the treated sample with dose of  $1 \times 10^{16}$  ions/cm<sup>2</sup>. A survey of the literatures [2, 8, 53] shows that the higher impedance

at low frequency (100 mHz) reflects slower charge transfer process. Fig 6 (d) shows the Bode phase angle evolution process of the untreated and treated sample. The maximum phase angles of the samples are -41.5 degrees (bare sample), -56.2

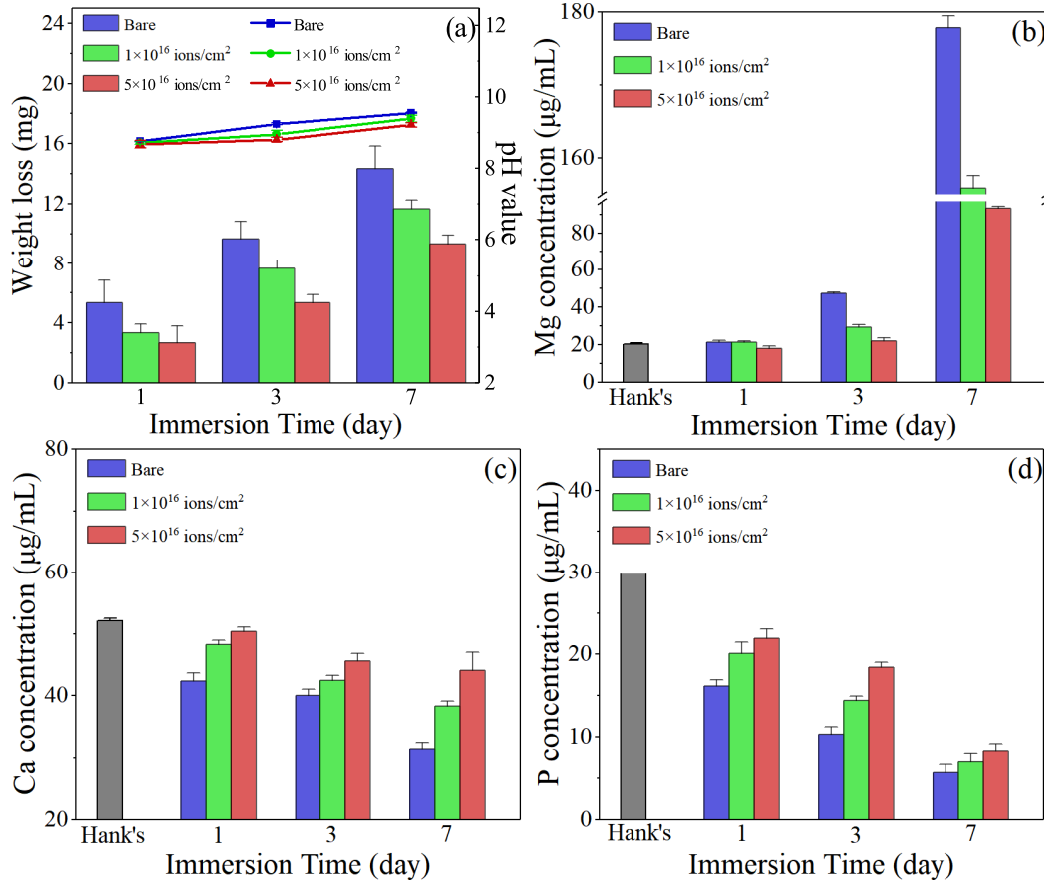


FIG. 8: (a) The pH values extracted from the Hank's solution and the weight loss after immersion for 1, 3, 7 days. And the concentrations of (b) Mg, (c) Ca, and (d) P after immersion for 1, 3, 7 days.

degrees (treated sample with dose of  $1 \times 10^{16}$  ions/cm<sup>2</sup>), and -57.9 degrees (treated sample with dose of  $5 \times 10^{16}$  ions/cm<sup>2</sup>), respectively. More capacitive behavior is demonstrated by larger phase angles of the treated samples, which suggests the formation of a more stable and dense layer to retard the electrolyte penetration into the substrate [11, 29, 33, 37, 48]. Hence, the Bode diagram confirms that corrosion resistance of the alloy is improved by the carboxyl ion implantation.

The electrical equivalent circuit is employed to fit the EIS spectra (Fig. 6 (b)). The fitted results are plotted as solid lines throughout the Nyquist and Bode plots as shown in Fig. 6 (a, c, d). Their corresponding EIS parameters derived from curve fitting are listed in Table II.  $R_s$  is the solution resistance between the working electrode and reference electrode.  $CPE_1$  represents the constant phase element of the outer porous layer, and  $R_p$  is the corresponding resistance.  $CPE_2$  stands for the constant phase element in the inner layer and in parallel with the resistance  $R_2$ . From Table II,  $R_s$  maintains relatively unchanged for different compositions of the samples in the same solution. As reported that the CPE value is related to the ability of the electrolytes to permeate into the porous surface layer [5, 38]. A decrease of CPE suggests that it is difficult to pass through the porous/defective surface layer for electrolytes. The values of  $R_1$  and  $R_2$  increase with the decreasing of  $CPE_1$  and  $CPE_2$  for the treated samples compared

to the untreated sample, which indicates the lower penetration rate of the Hank's solution into the treated sample surface. Moreover,  $R_1$  has a significantly lower value than  $R_2$  for the untreated sample. It implies the formation of the thin porous outer layer, which can not suppress the transfer of the corrosive chloride ions and other chemical compounds. So the magnesium substrate of the untreated sample is easily attacked by the abundant chloride ions. On the other hand, the significantly higher values of  $R_1$  and  $R_2$  of the treated samples are due to the formation of carboxylic group, carbonates, metal oxides and hydroxides on the surface layer after carboxyl ion implantation. Thus the formed compact and protective structure on the surface of the treated sample possess a barrier to protect the ZK60 Mg alloy from corrosion. The above EIS results suggest that the treated samples effectively improve the corrosion resistance and are well consistent with the polarization curve.

To further evaluate the corrosion behavior, the corrosion morphologies of the untreated and treated samples are analyzed with SEM, as shown in Fig. 7. The samples were soaked in the Hank's solution at 37°C for 1, 3, and 7 days, respectively. Plenty of cracks are viewed on the surface for the untreated sample, and the crack spacing propagates obviously with the immersion time, as shown in Group a in Fig. 7. Severe large corrosion pits emerge on the untreated sample

TABLE II: Electrochemical parameters derived from the equivalent circuit models.

Parameters	Bare	$1 \times 10^{16}$	$5 \times 10^{16}$
$R_s (\Omega cm^2)$	20	19.363	19.12
$R_1 (\Omega cm^2)$	15.849	360.8	338.9
$R_2 (\Omega cm^2)$	253.47	496.68	950.49
$CPE_1 - T (\Omega^{-2} cm^2 S^{-n})$	$5 \times 10^{-4}$	$4.8789 \times 10^{-4}$	$4.3942 \times 10^{-4}$
$CPE_1 - P$	0.363	0.63736	0.8271
$CPE_2 - T (\Omega^{-2} cm^2 S^{-n})$	$5.1949 \times 10^{-5}$	$3.1653 \times 10^{-5}$	$3.0092 \times 10^{-5}$
$CPE_2 - P$	0.85261	0.88782	0.84661

surface after immersion for 7 days, which specifies its highest corrosion rate. On the other hand, for the treated samples with dose of  $5 \times 10^{16}$  ions/cm<sup>2</sup>, except some eroding cracks and pits, their surfaces haven't undergone visible damage. The treated samples display smaller crack spacing compared with untreated sample after immersion for 7 days. Thus, the corrosion of the ZK60 Mg alloy is effectively suppressed by the COOH<sup>+</sup> implantation on the surface.

Additionally, Fig. 8 shows the weight loss, the pH value measured from the Hank's solution, and the released ion concentrations of Mg, Ca, P of the untreated and treated samples. As shown in Fig. 8 (a), the tendency of the continuous increase of the weight loss of the samples is observed with longer immersion time. The untreated sample exhibits larger weight loss compared with the treated sample at each time node. For the treated samples, the weight loss decreases with increasing the implantation dose, indicating the superior corrosion resistance for the treated sample with higher dose. Similar case is observed in the pH values of the untreated and treated samples. The untreated sample has slightly higher pH values, which suggests a higher corrosion rate. As shown in Fig. 8 (b-d), the release of Mg ion increases gradually over the immersion time. The treated sample dissolves less Mg ion in the corrosive solution than the untreated sample. The lowest dissolution of Mg is found for the sample implanted by the COOH<sup>+</sup> with dose of  $5 \times 10^{16}$  ions/cm<sup>2</sup>. After immersion for 7 days, the concentrations of Ca and P in the solution extracted by the untreated sample are  $31.33 \pm 1.04 \mu\text{g/mL}$  and  $5.73 \pm 0.95 \mu\text{g/mL}$ , lower than the treated sample with dose of  $5 \times 10^{16}$  ions/cm<sup>2</sup> (Ca:  $44.10 \pm 2.92 \mu\text{g/mL}$  and P:  $0.27 \pm 0.83 \mu\text{g/mL}$ ). The results are attributed to the more insoluble Ca and P corrosion products formed for the untreated sample in the corrosion process. Therefore, the degradation rate of the treated sample is lower than the untreated sample. These results are in consistent with the analyses of the surface morphology, and all the corrosion assays indicate that the corrosion behavior is effectively enhanced after the carboxyl ion implantation.

#### D. *In vitro* cytotoxicity studies

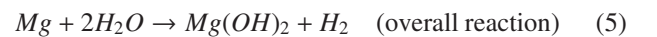
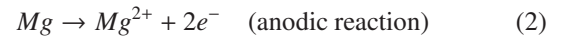
The *in vitro* cytotoxicity of the untreated and the treated ZK60 Mg alloys are evaluated by measuring the viability of MC3T3-E1 cells after culturing for 3 days in the extracts with different concentrations (20%, 50%, 70%, and 100%). In the light of ISO 10993-5 [1, 45], if the cell viability exceeds 80%,

the biological material exhibits none or slight cytotoxicity; if the cell viability ranges from 50% to 79%, it exhibits mild cytotoxicity; if the cell viability is between 30% and 49%, it exhibits moderate cytotoxicity; if the cell viability is below 30%, it exhibits severe cytotoxicity. As shown in Fig. 9, both the untreated and the treated samples have relatively low cell viability in the extract with concentration of 100% after being incubated for 3 days. The cell viability of the untreated sample does not reach more than 80% until the extract concentration reduces to 20%, suggesting the severe toxicity effect. However, the cell viability increases gradually as reducing the extract concentration. The cell viability has grown to over 80% for the implanted alloy with dose of  $5 \times 10^{16}$  ions/cm<sup>2</sup> when the extract concentration is 70%, showing a good cytocompatibility. All the treated samples with different implantation doses achieve high cell viability above 80% when the extract concentration is less than 50%. Additionally, the cell viability of the treated sample with dose of  $5 \times 10^{16}$  ions/cm<sup>2</sup> is visibly larger than that of the dose of  $1 \times 10^{16}$  ions/cm<sup>2</sup>. This is caused by that the treated sample with dose of  $5 \times 10^{16}$  ions/cm<sup>2</sup> has lower degradation rate making for less ion dissolution in the extract solution. Overall, the MC3T3-E1 cells grown in the extract of treated samples present significantly higher activity than that of the untreated sample for the whole extract concentration during the whole incubation period, indicating that the cytotoxic effect is restrained owing to the ion implantation into the alloy surface.

## IV. DISCUSSION

### A. Corrosion behavior

The magnesium corrosion mechanism has been reported in literatures [12, 41, 42], the degradations of the Mg alloys involve the electrochemical reactions, which correspond to the metal dissolution at the anodic, and the oxygen reduction at the cathodic, as shown in the following chemical equations:



With respect to the untreated sample, magnesium dissolves rapidly in Hank's solution filled with plenty of chloride ions, which results in the increase of Mg<sup>2+</sup> concentration at anodic electrode. Simultaneously, OH<sup>-</sup> ions are accumulated at cathodic electrode where the local high alkalinity is produced (Eq. (3)). The low soluble Mg hydroxide formed by the reaction of Mg<sup>2+</sup> and OH<sup>-</sup> (Eq. (4)) precipitates on the alloy

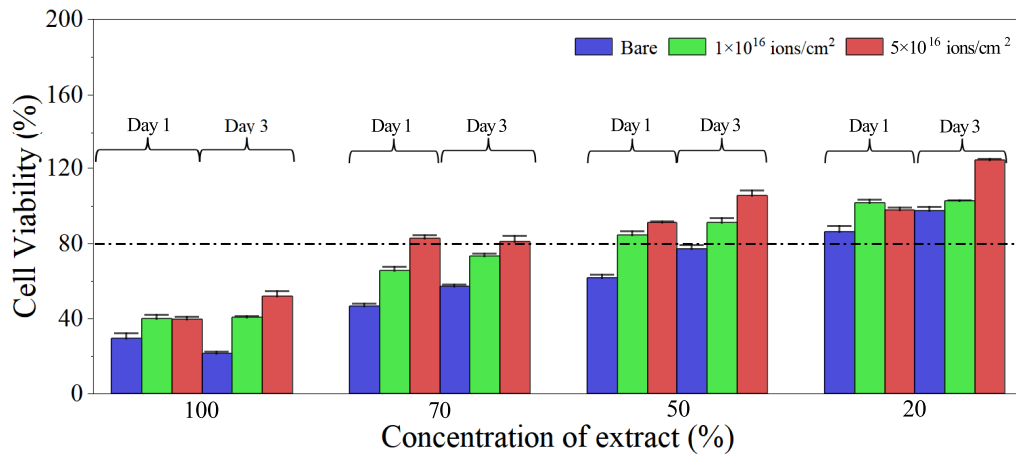


FIG. 9: *In vitro* viability of MC3T3-E1 cells cultured in the different concentration extracts of bare and treated samples for 1 and 3 days.

surface to serve as the initial barrier against the solution penetration. However, this  $Mg(OH)_2$  layer is too loose, porous, and unstable to protect the substrate when encountering with abundant chloride ions in the solution. Then the non-uniform  $Mg(OH)_2$  is converted into  $MgCl_2$  further lessening the protection. Thus, the Mg substrate underneath the porous corrosion product is readily corroded by the electrolyte. The increase in corrosion current density and the decrease in EIS nyquist arc suggest that the porous surface layer is unable to stop the electrolyte permeation on the untreated sample. As the corrosion progresses, the Mg phosphate and carbonate are formed by consuming the Ca and P ions in the corrosion solution. The degradation of the ZK60 alloy leads to the increased amount of Mg ions and the decreased Ca and P ions in the solution. The results of higher Mg concentration and lower Ca and P concentrations are shown in Fig. 8, which indicates the impaired corrosion resistance of the untreated sample.

However, for the treated sample, the formation of the stable barrier layer containing carboxylic group, Mg carbonates, metal oxides and hydroxides effectively retards the electrolyte penetration into the alloy. Both the higher  $R_1$  and  $R_2$  resistance values in the EIS analysis confirm the improved corrosion resistance of the treated sample. Additionally, the  $R_2$  is significantly higher than  $R_1$ , implying that the corrosion resistance is indeed dominated by the barrier layer formed by the carboxylic ion implantation. It is noted that most of the surface areas are well protected by the barrier layer, while corrosion in some regions can be identified by examining the surface morphology (Fig. 7), which can be explained as that the barrier layer is not homogeneously covers the whole alloy surface.

The concentration change by ICP-OES support the corrosion resistance. The corrosion products, such as the Mg carbonate and phosphate, are formed by consuming Ca and P ions. Hence, the Mg concentration rises, whereas Ca and P concentrations decline, which verifies the formation of local alkaline environment. In comparison with the bare sample, the treated sample exhibits lower Mg concentration and higher Ca and P concentrations, which reveals the reduced degradation rate. Overall, the corrosion rate is significantly reduced

after the grafting of carboxyl group on the surface of ZK60 Mg alloy.

## B. Cytotoxicity evaluation

The mouse osteoblast MC3T3 cells are used to evaluate the effect of the carboxyl ion implantation on cytotoxicity into the ZK60 Mg alloy. The Mg alloy can gradually dissolves in the physiological environment after being implanted into the living body as the osteosynthesis material. The degradation process leads to the increase in the pH value generating the local alkaline environment [31]. The obvious cytotoxic effect is occurred when the amount of the released ions from the implanted objects are beyond the maximum dosage tolerated by the tissues. As reported in literature [51], the viability of MC3T3-E1 cells is significantly facilitated when the extract medium contains 50  $\mu\text{g/ml}$  Mg ions, whereas the reduced viability is observed when the Mg ion concentration exceeds 200  $\mu\text{g/ml}$ . In this study, for 3 day culture period, the cell viability is smaller than 30% for the untreated sample with extract at 100%, encountering severe toxic effects as shown in Fig. 9. The cell viability keeps at a low level although there is an increase trend with diluted extract. This implies that the high degradation rate of the untreated sample produces the high Mg concentration above the tolerance level, and in this alkaline environment, hydrogen gas accumulates surrounds the host tissue, leading to the necrosis and separation of tissues [40, 43]. Some studies have reported the similar results about the presence of cytotoxic effects of Mg-Zn alloys. Jin et al. [21] demonstrated that the extremely low viability of the MC3T3-E1 pre-osteoblasts was found in 70% extract of ZK60 Mg alloy. Hong et al. [16] also reported that the ZK40 Mg alloy possesses almost tiny cell viability with undiluted extract. On the other hand, the treated samples have not induced obvious toxicity to MC3T3-E1 cells cultured with 70% extract after the incubation for 3 days. This demonstrates that the reduced corrosion rate leads to the limited alkalization and hydrogen evolution to slow the release of ions from the Mg implants. In addition, the carboxyl functional group

facilitates the cell attachment and proliferation due to its less toxic than metal ions [23, 54]. The carboxylic ion implantation which promotes the formation of a relatively smooth and functional surface layer containing carboxylic group, carbonates, metal oxides and hydroxides on the substrate surface has shown obvious advantage in corrosion resistance, biocompatibility, and mechanical behavior. All of these are vital factors for materials in clinical applications.

## V. CONCLUSIONS

In this study, ZK60 magnesium alloy is implanted by carboxylic ions with the doses of  $1 \times 10^{16}$  and  $5 \times 10^{16}$  ions/cm<sup>2</sup> at energy of 200 KeV. The performance of mechanical behavior, degradation rate and *in vitro* cytotoxicity are systematically investigated. The surface mechanical performance of surface modified alloy is improved after the ion implantation, which is confirmed by the Nano Indenter experiment. The treated samples exhibit the reduced corrosion rate which is demonstrated by the experimental results in the potentiodynamic po-

larization, electrochemical impedance spectroscopy, and the immersion analyses. The improvement can be attributed to the smoother surface layer containing various carbonates, metal oxides and hydroxides compound as a passive barrier layer to prevent the penetration of the corrosive solution. The *in vitro* cytotoxicity experiment using osteoblast MC3CT3 cell shows the higher viability of the treated samples with the promising biocompatibility. Although this is only a preliminary study on the grafting of carboxyl onto magnesium alloys, this study provides a perspective of employing the organic functional groups implantation techniques to improve the biodegradable magnesium alloys.

## ACKNOWLEDGMENTS

This work is supported by National Science Foundation (NSF) of China with the Grant No.11675014. Additional support is provided by Ministry of Science and Technology of China (2013YQ030595 – 3).

- 
- [1] ISO 10993-5:2009(E). *Biological evaluation of medical devices*. Part 5: Tests for in vitro cytotoxicity. International Organization for Standardization, 2009.
- [2] A Amirudin and D Thieny. Application of electrochemical impedance spectroscopy to study the degradation of polymer-coated metals. *Progress in organic coatings*, 26(1):1–28, 1995.
- [3] Sara Bagherifard, Daniel J Hickey, Stanislava Fintová, Filip Pastorek, Ines Fernandez-Pariente, Michele Bandini, Thomas J Webster, and Mario Guagliano. Effects of nanofeatures induced by severe shot peening (ssp) on mechanical, corrosion and cytocompatibility properties of magnesium alloy az31. *Acta biomaterialia*, 66:93–108, 2018.
- [4] G Ballerini, K Ogle, and M-G Barthés-Labrousse. The acid-base properties of the surface of native zinc oxide layers: an xps study of adsorption of 1, 2-diaminoethane. *Applied surface science*, 253(16):6860–6867, 2007.
- [5] F Bellucci and L Nicodemo. Water transport in organic coatings. *Corrosion*, 49(3):235–247, 1993.
- [6] M Bolduc, D Popovici, and B Terreault. Deep segregation and hardening in al-mg-zn-cu-cr alloy treated by plasma source oxygen ion implantation. *Surface and Coatings Technology*, 138(2-3):125–134, 2001.
- [7] Kasey Catt, Huaxiu Li, and X Tracy Cui. Poly (3, 4-ethylenedioxythiophene) graphene oxide composite coatings for controlling magnesium implant corrosion. *Acta biomaterialia*, 48:530–540, 2017.
- [8] Y Chen, XH Wang, J Li, JL Lu, and FS Wang. Long-term anticorrosion behaviour of polyaniline on mild steel. *Corrosion science*, 49(7):3052–3063, 2007.
- [9] Yu Qiang Chen, Fu Yi Gao, Hong Yan Peng, Hong Wei Jiang, Long Cheng Yin, Dan Wang, and Hai Liang Huang. Deposition of titanium nitride film on mg-li alloys by dc reactive magnetron sputtering. In *Advanced Materials Research*, volume 204, pages 1685–1690. Trans Tech Publ, 2011.
- [10] AB Christie, I Sutherland, and JM Walls. An xps study of ion-induced dissociation on metal carbonate surfaces. *Vacuum*, 31(10-12):513–517, 1981.
- [11] Sergio Luiz de Assis, Stephan Wolyneec, and Isolda Costa. Corrosion characterization of titanium alloys by electrochemical techniques. *Electrochimica Acta*, 51(8-9):1815–1819, 2006.
- [12] Amos Doepke, Dingchuan Xue, Yeoheung Yun, William J Vanooij, H Brian Halsall, and William R Heineman. Corrosion of organosilane coated mg4y alloy in sodium chloride solution evaluated by impedance spectroscopy and ph changes. *Electrochimica Acta*, 70:165–170, 2012.
- [13] Ronald J Elin. Assessment of magnesium status for diagnosis and therapy. *Magnesium research*, 23(4):194–198, 2010.
- [14] DongMei Gao, JingBo Hu, Meng Yang, and QiLong Li. Determination of daunomycin at a novel cooh/indium tin oxide ion implantation-modified electrode. *Analytical biochemistry*, 358(1):70–75, 2006.
- [15] Daniel J Hickey, Batur Ercan, Linlin Sun, and Thomas J Webster. Adding mgo nanoparticles to hydroxyapatite–plla nanocomposites for improved bone tissue engineering applications. *Acta biomaterialia*, 14:175–184, 2015.
- [16] Daeho Hong, Partha Saha, Da-Tren Chou, Boeun Lee, Boyce E Collins, Zongqing Tan, Zhongyun Dong, and Prashant N Kumta. In vitro degradation and cytotoxicity response of mg–4% zn–0.5% zr (zk40) alloy as a potential biodegradable material. *Acta biomaterialia*, 9(10):8534–8547, 2013.
- [17] T Hong and M Nagumo. Effect of surface roughness on early stages of pitting corrosion of type 301 stainless steel. *Corrosion science*, 39(9):1665–1672, 1997.
- [18] ASTM Internasional. Astm g31-72: Standart practice for laboratory immersion corrosion testing of metals. *United State*, 2004.
- [19] M Jamesh, Guosong Wu, Ying Zhao, and Paul K Chu. Effects of silicon plasma ion implantation on electrochemical corrosion behavior of biodegradable mg–y–re alloy. *Corrosion Science*, 69:158–163, 2013.
- [20] Mohammed Ibrahim Jamesh, Guosong Wu, Ying Zhao, David R McKenzie, Marcela MM Bilek, and Paul K Chu. Effects of zirconium and oxygen plasma ion implantation on the corrosion behavior of zk60 mg alloy in simulated body fluids.

- Corrosion Science*, 82:7–26, 2014.
- [21] Weihong Jin, Guomin Wang, Zhengjie Lin, Hongqing Feng, Wan Li, Xiang Peng, Abdul Mateen Qasim, and Paul K Chu. Corrosion resistance and cytocompatibility of tantalum-surface-functionalized biomedical zirconium alloy. *Corrosion Science*, 114:45–56, 2017.
- [22] NT Kirkland, Nick Birbilis, and MP Staiger. Assessing the corrosion of biodegradable magnesium implants: a critical review of current methodologies and their limitations. *Acta biomaterialia*, 8(3):925–936, 2012.
- [23] DJ Li and LF Niu. Cell attachment of polypropylene surface-modified by cooh<sup>+</sup> ion implantation. *Nuclear Instruments and Methods in Physics Research Section B: Beam Interactions with Materials and Atoms*, 192(4):393–401, 2002.
- [24] Nan Li and Yufeng Zheng. Novel magnesium alloys developed for biomedical application: a review. *Journal of Materials Science & Technology*, 29(6):489–502, 2013.
- [25] Shuoqi Li, Wei Cao, Ji Xia, Jingbo Hu, and Qilong Li. Cooh<sup>+</sup> ion implantation-modified indium tin oxide electrode for the direct electrochemistry of cytochrome c. *Nuclear Instruments and Methods in Physics Research Section B: Beam Interactions with Materials and Atoms*, 268(13):2235–2240, 2010.
- [26] Shuoqi Li, Ji Xia, Chenyao Liu, Yanzhen Zheng, Lu Zeng, Jingbo Hu, and Qilong Li. Direct electrochemistry and electrocatalysis of hemoglobin on an indium tin oxide electrode modified with implanted carboxy ions. *Microchimica Acta*, 167(1-2):41, 2009.
- [27] W Li and DY Li. Influence of surface morphology on corrosion and electronic behavior. *Acta materialia*, 54(2):445–452, 2006.
- [28] Jiao Liu, Yang Zheng, Yanze Bi, Yan Li, and Yufeng Zheng. Improved cytocompatibility of mg-1ca alloy modified by zn ion implantation and deposition. *Materials Letters*, 205:87–89, 2017.
- [29] John N Murray. Electrochemical test methods for evaluating organic coatings on metals: an update. part iii: Multiple test parameter measurements. *Progress in Organic coatings*, 31(4):375–391, 1997.
- [30] Ming Ni and Buddy D Ratner. Differentiating calcium carbonate polymorphs by surface analysis techniques: xps and tof-sims study. *Surface and Interface Analysis: An International Journal devoted to the development and application of techniques for the analysis of surfaces, interfaces and thin films*, 40(10):1356–1361, 2008.
- [31] Toshiaki Ohtsuka. Corrosion protection of steels by conducting polymer coating. *International Journal of Corrosion*, 2012, 2012.
- [32] Ashish Pandey and Anjum Qureshi. Surface modified graphene oxide nanosheets by gold ion implantation as a substrate for surface enhanced raman scattering. *Journal of Alloys and Compounds*, 703:500–507, 2017.
- [33] JH Park, GD Lee, A Nishikata, and T Tsuru. Anticorrosive behavior of hydroxyapatite as an environmentally friendly pigment. *Corrosion Science*, 44(5):1087–1095, 2002.
- [34] RWY Poon, KWK Yeung, XY Liu, PK Chu, CY Chung, WW Lu, KMC Cheung, and D Chan. Carbon plasma immersion ion implantation of nickel–titanium shape memory alloys. *Biomaterials*, 26(15):2265–2272, 2005.
- [35] G Ruhi, OP Modi, and IB Singh. Corrosion behaviour of nano structured sol-gel alumina coated 9cr–1mo ferritic steel in chloride bearing environments. *Surface and Coatings Technology*, 204(3):359–365, 2009.
- [36] K Sasaki and GT Burstein. The generation of surface roughness during slurry erosion-corrosion and its effect on the pitting potential. *Corrosion Science*, 38(12):2111–2120, 1996.
- [37] A Shi, S Koka, and J Ullett. Performance evaluation on the weathering resistance of two usaf coating systems (standard 85285 topcoat versus fluorinated apc topcoat) via electrochemical impedance spectroscopy. *Progress in organic coatings*, 52(3):196–209, 2005.
- [38] IB Singh, DP Mandal, M Singh, and S Das. Influence of sic particles addition on the corrosion behavior of 2014 al–cu alloy in 3.5% nacl solution. *Corrosion Science*, 51(2):234–241, 2009.
- [39] IB Singh, M Singh, and S Das. A comparative corrosion behavior of mg, az31 and az91 alloys in 3.5% nacl solution. *Journal of Magnesium and Alloys*, 3(2):142–148, 2015.
- [40] Guangling Song. Control of biodegradation of biocompatible magnesium alloys. *Corrosion science*, 49(4):1696–1701, 2007.
- [41] Guangling Song and Andrej Atrens. Understanding magnesium corrosion: a framework for improved alloy performance. *Advanced engineering materials*, 5(12):837–858, 2003.
- [42] Guangling Song, Andrej Atrens, and Matthew Dargusch. Influence of microstructure on the corrosion of diecast az91d. *Corrosion science*, 41(2):249–273, 1998.
- [43] Mark P Staiger, Alexis M Pietak, Jerawala Huadmai, and George Dias. Magnesium and its alloys as orthopedic biomaterials: a review. *Biomaterials*, 27(9):1728–1734, 2006.
- [44] Xue Wei Tao, Zhang Zhong Wang, Xiao Bo Zhang, Zhi Xin Ba, and Ya Mei Wang. Nanomechanical and corrosion properties of zirconium magnesium alloy improved by gd ion implantation. *Surface Review and Letters*, 21(06):1450085, 2014.
- [45] Xian Tong, Dechuang Zhang, Xiaotuan Zhang, Yingchao Su, Zimu Shi, Kun Wang, Jianguo Lin, Yuncang Li, Jixing Lin, and Cuie Wen. Microstructure, mechanical properties, biocompatibility, and in vitro corrosion and degradation behavior of a new zn–5ge alloy for biodegradable implant materials. *Acta biomaterialia*, 82:197–204, 2018.
- [46] Zia ur Rahman, KM Deen, Lawrence Cano, and Waseem Haider. The effects of parametric changes in electropolishing process on surface properties of 316l stainless steel. *Applied Surface Science*, 410:432–444, 2017.
- [47] GJ Wan, MF Maitz, H Sun, PP Li, and N Huang. Corrosion properties of oxygen plasma immersion ion implantation treated magnesium. *Surface and Coatings Technology*, 201(19-20):8267–8272, 2007.
- [48] ZB Wang, HX Hu, CB Liu, and YG Zheng. The effect of fluoride ions on the corrosion behavior of pure titanium in 0.05 m sulfuric acid. *Electrochimica acta*, 135:526–535, 2014.
- [49] Frank Witte, Norbert Hort, Carla Vogt, Smadar Cohen, Karl Ulrich Kainer, Regine Willumeit, and Frank Feyerabend. Degradable biomaterials based on magnesium corrosion. *Current opinion in solid state and materials science*, 12(5-6):63–72, 2008.
- [50] Frank Witte, V Kaese, H Haferkamp, E Switzer, A Meyer-Lindenberg, CJ Wirth, and H Windhagen. In vivo corrosion of four magnesium alloys and the associated bone response. *Biomaterials*, 26(17):3557–3563, 2005.
- [51] Hoi Man Wong, Shuilin Wu, Paul K Chu, Shuk Han Cheng, Keith DK Luk, Kenneth MC Cheung, and Kelvin WK Yeung. Low-modulus mg/pcl hybrid bone substitute for osteoporotic fracture fixation. *Biomaterials*, 34(29):7016–7032, 2013.
- [52] Zhigang Xie, Adolph Miller Allen, Mei Chang, Phillip Wang, and Tza-jing Gung. Control of bombardment energy and energetic species toward a superdense titanium nitride film. *Journal of Vacuum Science & Technology A: Vacuum, Surfaces, and Films*, 28(6):1326–1329, 2010.
- [53] Ruizhen Xu, Xiongbo Yang, Penghui Li, Kai Wong Suen, Guosong Wu, and Paul K Chu. Electrochemical properties and corrosion resistance of carbon-ion-implanted magnesium. *Corrosion Science*, 82:173–179, 2014.
- [54] Yiteng Zhang, Minsi Li, Mengli Zhao, and Dejun Li. Influence of polar functional groups introduced by cooh<sup>+</sup> implantation on

- cell growth and anticoagulation of mwcnts. *Journal of Materials Chemistry B*, 1(41):5543–5549, 2013.
- [55] Tingting Zhao, Yan Li, Yong Liu, and Xinqing Zhao. Nano-hardness, wear resistance and pseudoelasticity of hafnium implanted niti shape memory alloy. *journal of the mechanical behavior of biomedical materials*, 13:174–184, 2012.
- [56] Ying Zhao, Mohammed Ibrahim Jamesh, Wing Kan Li, Guosong Wu, Chenxi Wang, Yufeng Zheng, Kelvin WK Yeung, and Paul K Chu. Enhanced antimicrobial properties, cytocompatibility, and corrosion resistance of plasma-modified biodegradable magnesium alloys. *Acta biomaterialia*, 10(1):544–556, 2014.